Geophys. J. Int. (2001) **145,** 749–758

Scattering and diffraction of *SH* waves by a finite crack: an analytical solution

Francisco J. Sánchez-Sesma[1] and Ursula Iturrarán-Viveros[2]

[1] *Instituto de Ingeniería, UNAM, Cd. Universitaria, Apdo* 70-472, *Coyoacán* 04510, *México. E-mail: sesma@servidor.unam.mx*
[2] *Instituto Mexicano del Petróleo, Eje Central L. Cárdenas* 152, CP 07730, *México. E-mail: uiturrar@imp.mx*

Accepted 2001 January 19. Received 2001 January 2; in original form 2000 June 13

SUMMARY

The diffraction of *SH* waves by a finite plane crack is studied. The classical Sommerfeld solution for a semi-infinite straight reflecting screen is used as a building block to calculate the diffracted field generated by a finite crack. The solution is derived from the analysis of the behaviour of diffracted waves. These waves, which are first generated at the edges of the crack, travel along the surfaces and are diffracted/reflected at the opposite edge. By iteratively taking into account the contribution to the total field of these travelling waves, an infinite series with a known limit is constructed, leading to an approximate analytical solution for the case of a finite plane crack. This solution is virtually exact for large frequencies and it is very good for incoming wavelengths of up to four times the size of the crack. Since the solution is explicit the computational cost is very low. Both frequency and time-domain results are included.

Key words: cracks, diffraction, radiation patterns, scattering, wave propagation.

1 INTRODUCTION

The problem of scattering and diffraction of elastic waves by cracks or inclusions has gained importance recently as a result of their emerging applications in seismology and geophysics. For instance, in the petroleum industry, one of the most relevant features of naturally fractured reservoirs is the extensive presence of cracks. Their detection and characterization is crucial for efficient oil production and recovery. When assuming that the radii of separation between cracks are small compared to the wavelength and interactions between cracks are negligible, one can use statistical hypotheses or homogenization techniques to differentiate diffraction patterns caused by many cracks from that of a single crack (see e.g. Hudson 1986). This highlights the importance of knowing the diffraction caused by a finite crack. This paper deals with scattering and diffraction of *SH* waves produced by the presence of an isolated 2-D crack within an infinite isotropic and homogeneous elastic medium.

The problem of scattering from a finite length crack is an old one, hence the existing literature on it is vast. All previous work approached the problem numerically. For instance, Loeber & Sih (1968) developed an integral transform method to obtain dynamic stresses around a finite crack. They reduced the scattering problem to the numerical evaluation of a system of coupled integral equations. The problems of diffraction of vector elastic waves by a clamped strip or by a finite crack have been treated numerically in Ang & Knopoff (1964a,b). There is considerable literature on the diffraction of elastic waves by semi-infinite cracks (or half-planes); see e.g. Mow & Pao (1971). Reviews of studies of elastic wave propagation in media containing cracks can be found in Kraut (1976) and, from the point of view of asymptotic ray theory, in Achenbach *et al.* (1982). Boström (1987) studied the case of an interface crack between two homogeneous elastic half-spaces for the case of anti-plane strain. He used a direct integral equation method with the crack-opening displacement as the unknown and Chebyshev polynomials as expansion functions for his numerical approximation. Recently, the problem of scattering of *SH* waves by a finite crack has been addressed in various ways. For instance, Huang (1995) considered a finite crack embedded in a half-space. The dislocation density functions and the stress field due to such discontinuities are expressed as a system of integral equations. These equations are solved by Galerkin numerical schemes. A parallel work to this study is the one by De Hoop (2000), in which an analytical time-domain expression is given for the 2-D diffraction of *SH* waves by an imperfection of finite width. An interesting application of the analytical solution presented here could be to study scattering effects caused by distributed cracks as in Murai *et al.* (1995) but with the advantage of computational speed over all these numerical schemes. Hence the power of the present solution lays in its simplicity, which enables a fast computation.

The terms *scattering* and *diffraction* are used loosely as synonyms. The former is suitable to name waves scattered by an object (with an implicitly high-frequency meaning), whereas the latter refers to the waves that smooth out discontinuities of the geometrical wavefield (which are stronger at low frequencies). In our treatment, the diffracted field is computed

taking advantage of the geometrical structure of the original Sommerfeld problem. This solution allows for an easy computation of the crack-opening displacement (COD) (the difference between the displacements on the *illuminated* and on the *shaded* sides). The scattered far field can be computed by means of a representation theorem. When using a representation theorem for the case of a finite plane crack, the difference between displacements (on the illuminated and shaded sides) is computed analytically; the COD represents exactly this displacement difference.

In the next section a brief summary of Sommerfeld's (1949) classical solution for the screening half-plane is first presented. An expression for the total field is given. This is the starting point of our iterative solution for a finite crack. In Section 3, we form a finite crack by superimposing incident, reflected and diffracted fields from two semi-infinite cracks and construct the analytical solution from the known solution of the two semi-infinite cracks. To carry out this construct, we shall identify the diffracted fields on the shaded and on the illuminated sides of the crack and those generated at the two edges. In Section 4, some numerical results are presented for the total field at the crack in both frequency and time domains. The far-field radiation patterns are shown for various incidence angles and frequencies.

2 DIFFRACTION BY A SEMI-INFINITE CRACK

Scattered waves are generated when an obstacle of finite dimension interferes with incident waves. There are two properties to be considered when studying scattering of elastic waves due to a crack. First, displacements and/or stresses across the surfaces of the crack can be discontinuous. Second, its edges generate diffracted waves. From a theoretical point of view we will consider a crack as being a zero-thickness discontinuity in the interior of a 2-D elastic solid. The surfaces of the crack are taken as free surfaces where the traction vanishes. Both faces are thought of as occupying the same space.

A detailed derivation of Sommerfeld's original result is beyond the scope of this work. For further details the reader is referred to Sommerfeld (1949). A brief sketch of this classical solution is given below.

Time-harmonic waves of anti-plane strain are defined by a displacement in the y-direction of the form $v(x, z)\exp(-i\omega t)$, where $v(x, z)$ satisfies Helmholtz's equation $\nabla^2 v + k^2 v = 0$, ∇^2 being the 2-D Laplacian, $k = \omega/\beta$ being the wavenumber, ω being the angular frequency, $\beta = \sqrt{\mu/\rho}$ being the shear-wave velocity, μ being the shear modulus and ρ being the density.

Consider the intersection of a semi-infinite crack of uniform zero thickness with the xz-plane shown in Fig. 1(a). A plane wave of anti-plane strain, incident upon the crack, is defined by

$$v^{(\mathrm{i})} = v_0 \exp\left[ikx\sin\gamma - ikz\cos\gamma\right], \tag{1}$$

where γ is the angle of incidence as shown in Fig. 1. The time dependence $\exp(-i\omega t)$ is omitted hereafter. The presence of a crack gives rise to both diffracted and reflected fields. The total displacement field may thus be expressed in the form

$$v^{(\mathrm{t})} = v^{(\mathrm{i})} + v^{(\mathrm{r})} + v^{(\mathrm{d})}, \tag{2}$$

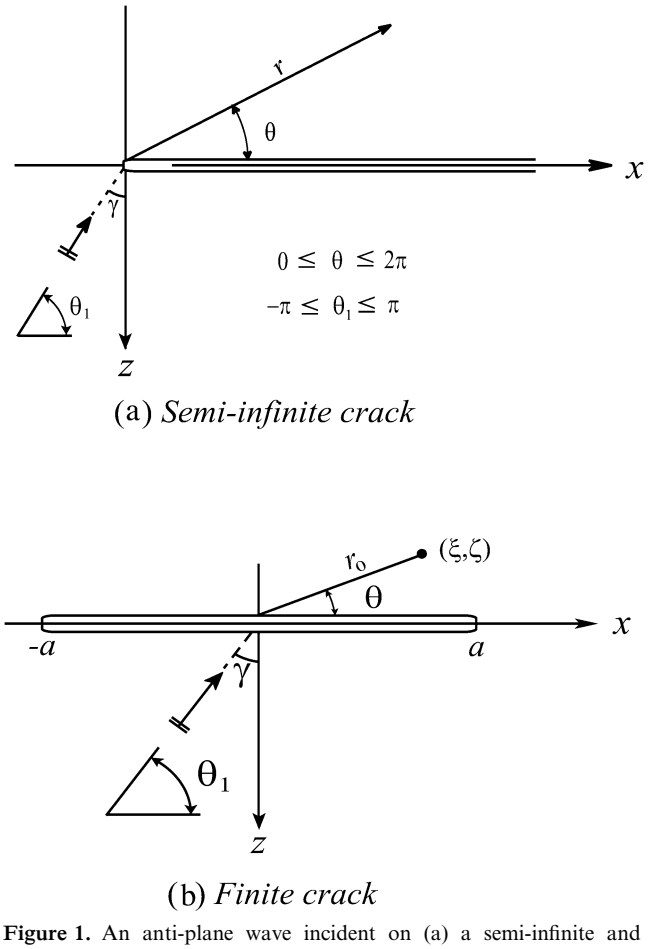

Figure 1. An anti-plane wave incident on (a) a semi-infinite and (b) a finite crack.

where $v^{(\mathrm{i})}$ is the incident wave, $v^{(\mathrm{r})}$ is the geometrical reflected wave and $v^{(\mathrm{d})}$ is the scattered field. Eq. (2) describes the overall effect generated by the presence of a crack for an incident wavefield. The field $v^{(\mathrm{t})}$ must satisfy the following:

(1) the Helmholtz equation;
(2) the crack faces are traction-free, thus we must have

$$\frac{\partial v^{(\mathrm{t})}}{\partial z} = 0\,, \quad x > 0\,, \quad z = 0\,; \tag{3}$$

(3) $v^{(\mathrm{t})}$ is finite and continuous everywhere, including the edge of the screen, but can be discontinuous across the screen (crack and screen are used synonymously);
(4) the edge of the screen neither radiates nor absorbs energy;
(5) the diffracted field $v^{(\mathrm{d})}$ must satisfy Sommerfeld's radiation condition at infinity.

For a perfectly reflecting plane screen the method of images leads to the problem of constructing branched solutions of the wave equation such that the edge of the screen is the branch line. Sommerfeld's classical solution to the diffraction problem is given by

$$v^{(\mathrm{t})} = W(r, \theta - \theta_1) + W(r, \theta + \theta_1)\,, \tag{4}$$

where the function $W(r, \theta - \theta_1)$ has a period 4π in the variable $\theta \pm \theta_1$.

In his work Sommerfeld proved that W in eq. (4) can be represented by a Fresnel integral in terms of a function $F(z)$

defined by

$$F(z) = \exp(-iz^2) \int_z^\infty \exp(i\tau^2) d\tau \,. \tag{5}$$

Further properties of function $F(z)$ can be found in Appendix A. Hence, the total field is given by

$$v^{(t)} = v_0 \frac{1}{\sqrt{\pi}} e^{i(kr-\pi/4)} \left\{ F\left[\sqrt{2kr} \sin\left(\frac{\theta_1 - \theta}{2}\right)\right] + F\left[\sqrt{2kr} \sin\left(\frac{\theta_1 + \theta}{2}\right)\right] \right\}, \tag{6}$$

which is the classical and well-known solution obtained by Sommerfeld for a semi-infinite crack. This solution is complete, thus it includes the incident, reflected and diffracted fields.

In the next section the COD and the scattered far field will be computed for a zero-thickness crack of length $2a$ based upon Sommerfeld's result.

3 FORMULATION OF THE PROBLEM

In this section Sommerfeld's solution is decomposed into a sum of the incident, reflected and diffracted fields. The idea is to superimpose the solution for a semi-infinite crack in the interval $(-a, +\infty)$ with the same solution for another semi-infinite crack in the interval $(-\infty, +a)$. Therefore, the finite crack (with edges at $x = \pm a$) could be thought of as occupying the space where the two semi-infinite cracks would intersect. Since Sommerfeld's formula is complete, when superimposing two solutions for two semi-infinite cracks the incident and reflected waves are repeated at the intersection of the two cracks and they will be eliminated. The symmetries of the generated fields are identified and exploited to build the solution for the finite crack. This construct is iterative and gives rise to a standard geometrical series, allowing the computation of the total field at the sides of the crack. We shall identify the side of the crack which is exposed to the incoming plane *SH* wave as the illuminated side (denoted by $+$); the other side is referred to as the shaded side (denoted by $-$). The geometry for the incidence of plane waves on a finite crack is depicted in Fig. 1(b).

The total displacement field $v^{(t)}$ for the finite crack is constructed as follows (see Fig. 2).

(i) Add the incident field $v^{(i)}$ everywhere as if there were no crack.

(ii) Add the reflected field $v^{(r)}$ with positive sign on the illuminated side and negative on the shaded side. This reflected field will cancel the incident field on the shaded side and will complete the geometric field $(v^{(i)} + v^{(r)})$ on the illuminated side.

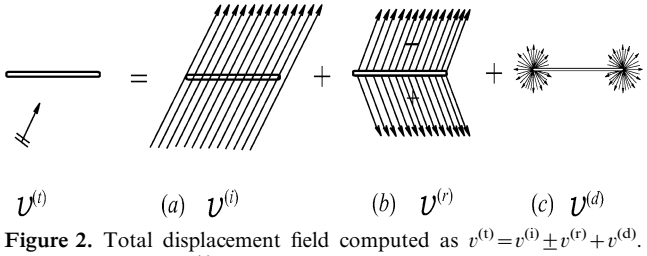

Figure 2. Total displacement field computed as $v^{(t)} = v^{(i)} \pm v^{(r)} + v^{(d)}$. The reflected field $v^{(r)}$ plays an important role in this formulation because on the shaded side (with the minus sign) it cancels out the incident field. On the other hand, on the illuminated side it completes the geometrical field.

(iii) Add the diffracted field $v^{(d)}$ produced at both edges of the crack.

This construct will allow us to find a simple expression for the diffracted field in the case of a finite crack. Let us define the following auxiliary function:

$$s(r) = \frac{2}{\sqrt{\pi}} e^{ikr - i\frac{\pi}{4}} \,. \tag{7}$$

On the shaded side there are neither incident nor reflected fields as they cancel each other. Therefore, the diffracted field coincides with the total field $v^{(d)-} = v^{(t)-}$. We shall compute the diffracted field on the shaded side (i.e. $\theta = 0$) generated at the edge $x = -a$ of a semi-infinite crack. According to Sommerfeld's formula, this is given by

$$v^{(t)^-} = v_0 e^{-ika \sin\gamma} s(r_1) F\left(\sqrt{2kr_1} \sin\frac{\theta_1}{2}\right), \tag{8}$$

where $r_1 = a + x$ and $\theta_1 = (\pi/2) - \gamma$. In order to compute the total field on the illuminated side (i.e. $\theta = 2\pi$), eq. (6) is again applied:

$$v^{(t)^+} = v_0 e^{-ika \sin\gamma} s(r_1) F\left(-\sqrt{2kr_1} \sin\frac{\theta_1}{2}\right). \tag{9}$$

Applying the property of $F(-z)$ given in eq. (A1) and using the following identity,

$$1 - 2\sin^2(\theta_1/2) = \cos(\theta_1) = \cos(\pi/2 - \gamma) = \sin\gamma \,, \tag{10}$$

eq. (9) yields

$$v^{(t)^+} = 2v_0 e^{ikx \sin\gamma} - v_0 e^{-ika \sin\gamma} s(r_1) F\left(\sqrt{2kr_1} \sin\frac{\theta_1}{2}\right) \tag{11}$$

at the illuminated side. The first term in eq. (11) is the incident field plus the reflected field $v^{(i)} + v^{(r)}$ (see Fig. 2) and the second term is the opposite of the diffracted field on the shaded side given in eq. (8). Therefore,

$$v^{(d)^+} = -v^{(d)^-} \,. \tag{12}$$

Hence, once the diffracted field is computed on the shaded side, the corresponding diffracted field on the illuminated side is immediately obtained. Since diffracted waves are generated at both edges of the crack, the same analysis is carried out for the right edge $(x = a)$. However, the reference system changes depending on whether we are considering the left or the right edge. As a result, when considering the edge at $x = a$ the incidence angle is $\theta_2 = (\pi/2 + \gamma)$ (see Fig. 3). Hence, a first approximation to the diffracted field on the shaded side generated by *SH* waves

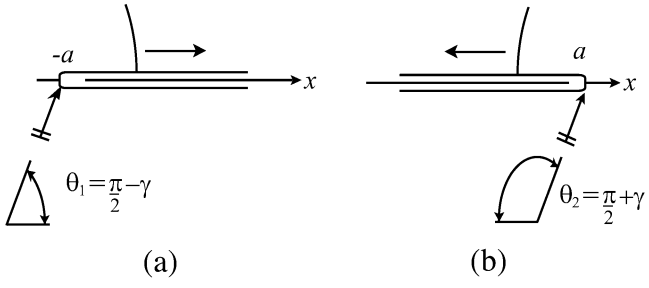

Figure 3. Diffracted waves caused by waves incident on the crack edges, travelling along the shaded side. (a) Reference system for the semi-infinite crack $(-a, +\infty)$. (b) As in (a) but for the semi-infinite crack $(-\infty, +a)$.

impinging on a finite crack is given by

$$v_0^{(d)^-} = v_0\, e^{-ika\sin\gamma} s(r_1)\, F\left(\sqrt{2kr_1}\sin\frac{\theta_1}{2}\right) + v_0\, e^{ika\sin\gamma} s(r_2)\, F\left(\sqrt{2kr_2}\sin\frac{\theta_1}{2}\right), \quad (13)$$

where $r_2 = a - x$ represents the waves travelling from right to left. The first term in eq. (13) corresponds to the scattered wave depicted in Fig. 3(a) and the second corresponds to Fig. 3(b). In order to have a better approximation, the next step is to consider the diffracted waves generated by interactions of both edges of the crack ($x = \pm a$). These are cylindrical waves that travel along the crack, reaching opposite edges impinging with an angle $\gamma \to \pm\pi/2$. The question that arises is under what circumstances these waves can be approximated as plane waves at the tips to compute the cylindrical waves reflected from the tips. This is a key point that deserves some explanation. Shortly after Sommerfeld had delivered his classical solution, Macdonald (1902) obtained series expansions in terms of Bessel functions for the total field in a wedge for both plane and cylindrical incoming waves. Macdonald's solutions include the limiting case of a half-plane, thus it is equivalent to Sommerfeld's formula. Now, let r be any point on the shaded side of the crack and consider a source point located on the illuminated side at a distance r_0 from the edge of the crack (see Fig. 4). Since we are interested in the case of a finite crack this source point will act as one of the edges (a diffracting point) and will be set to $r_0 = 2a$ (i.e. r_0 is the length of the crack). Macdonald's solution allows us to compare this case with Sommerfeld's result for a semi-infinite crack with an incidence γ that tends to $\pm\pi/2$. In Fig. 4 numerical comparisons show a very good agreement between these two solutions (results for four different frequencies are shown). Note that as the frequency decreases, the plane wave approximation for the actual cylindrical wave deteriorates. However, for such small frequencies the COD is very close to zero. This implies that even though the plane wave approximation deteriorates for low frequencies, the actual contribution of these frequencies to the COD is almost zero. Hence diffracted cylindrical waves that reach the edge have produced diffracted waves that can be very accurately approximated by those produced by grazing plane waves. We will keep this assumption in what follows. When the incoming plane wave reaches the edges, waves scattered (on the shaded side) have the form given in eq. (13). The new phase of the scattered wave at $x = -a$ is given by applying eq. (8) at $x = a$, i.e.

$$v_1 = v_0\, e^{-ika\sin\gamma} s(2a) F\left(\sqrt{4ka}\sin\frac{\theta_1}{2}\right). \quad (14)$$

Similarly, the new phase of the scattered wave at $x = a$ is given by applying eq. (8) at $x = -a$, i.e.

$$v_2 = v_0\, e^{ika\sin\gamma} s(2a) F\left(\sqrt{4ka}\sin\frac{\theta_2}{2}\right). \quad (15)$$

Using an equation similar to eq. (8), but with phase v_1 given by eq. (14) and letting $\theta_1 \to \pi$, the diffracted wave at $x = a$ is then given by

$$v_1' = v_1 s(r_2) F(\sqrt{2kr_2}). \quad (16)$$

In the same way for $x = -a$ we obtain

$$v_2' = v_2 s(r_1) F(\sqrt{2kr_1}). \quad (17)$$

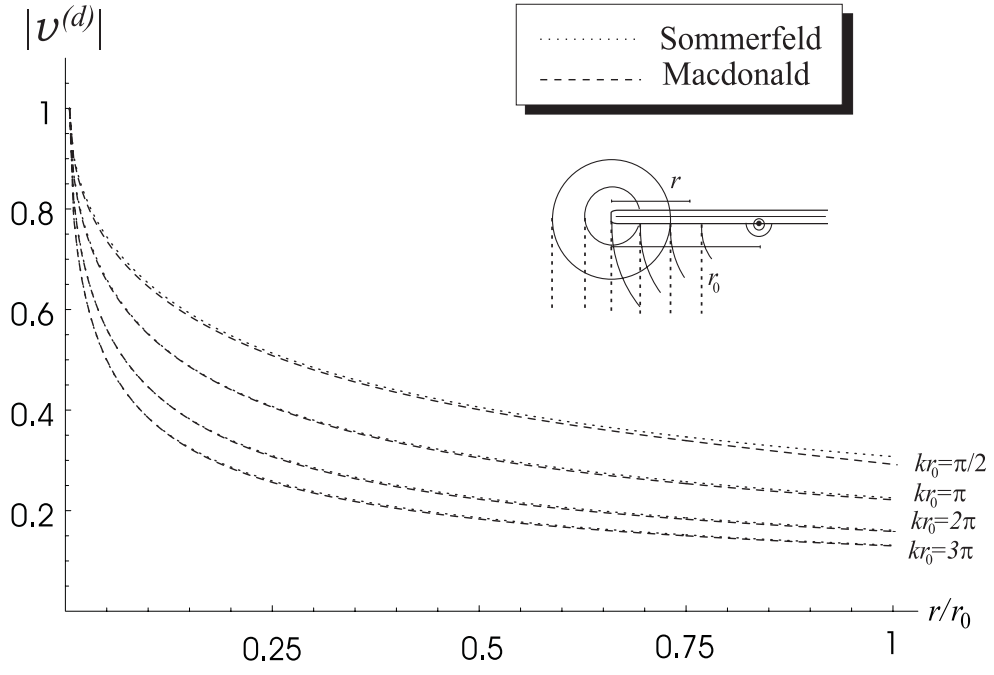

Figure 4. Comparison between diffracted cylindrical waves along the shaded side of the crack. They are calculated using Macdonald's solution and Sommerfeld's result for a plane wave with incident angle $\gamma = \pi/2$. Note that as the frequency decreases, the plane wave approximation for the actual cylindrical wave deteriorates. However, for such small frequencies the COD is very close to zero. This implies that even though the plane wave approximation deteriorates for low frequencies, the actual contribution of these frequencies to the COD is almost null.

When diffracted waves reach one of the edges $\theta_1=\pi$ or $\theta_2=\pi$, each of the reflected diffractions has a new amplitude and phase. It is necessary to multiply them by a factor Z given by

$$Z = s(2a)F(\sqrt{4ka})\,, \tag{18}$$

where function $s(x)$ is as defined in eq. (7). Factor Z takes into account the reflections due to diffracted waves on the illuminated side. The next step is to collect all the terms that correspond to diffracted waves travelling in both directions. The diffracted field can then be expressed as

$$\begin{aligned} v^{(\mathrm{d})^-} &= v_0^{(\mathrm{d})^-} \\ &+ v_1\Big\{\big[Z+Z^3+\ldots\big]s(r_1)F\Big(\sqrt{2kr_1}\Big) \\ &- \big[1+Z^2+\ldots\big]s(r_2)F\Big(\sqrt{2kr_2}\Big)\Big\} \\ &+ v_2\Big\{\big[Z+Z^3+\ldots\big]s(r_2)F\Big(\sqrt{2kr_2}\Big) \\ &- \big[1+Z^2+\ldots\big]s(r_1)F\Big(\sqrt{2kr_1}\Big)\Big\}\,, \end{aligned} \tag{19}$$

where $v_0^{(\mathrm{d})^-}$ is given by eq. (13).

From eqs (B1), (B2) and (B3) in Appendix B we conclude that if $ka>0$ then $|Z|<1$. Therefore, the series in eq. (19) are standard geometrical series with a known limit. Thus an analytical expression for the diffracted field can finally be obtained and this is given by rewriting eq. (19) as

$$\begin{aligned} v^{(\mathrm{d})^-} &= v_0^{(\mathrm{d})^-} + \frac{v_1Z-v_2}{1-Z^2}\,s(r_1)F(\sqrt{2kr_1}) \\ &+ \frac{v_2Z-v_1}{1-Z^2}\,s(r_2)F(\sqrt{2kr_2})\,, \end{aligned} \tag{20}$$

where $v_0^{(\mathrm{d})^-}$ is given by eq. (13). This analytical expression for the diffracted field on the shaded side of the crack, used in conjunction with the symmetries of the diffracted and reflected fields, allows us to describe completely the wave motion at both sides of the crack. An extension of eq. (20) to evaluate the fields away from the crack is a cumbersome task beyond the scope of this paper. Instead, we select a simpler, accurate approach based upon the Somigliana representation theorem.

Let us consider again a finite crack (zero thickness) of length $2a$. The displacement field under harmonic excitation can be written by means of the Somigliana representation theorem (see e.g. Achenbach 1973; Aki & Richards 1980; Banerjee & Butterfield 1981) as follows:

$$v^{(\mathrm{t})}(\boldsymbol{\xi}) = -\int_{-a}^{a} T^{+}(\mathbf{x},\boldsymbol{\xi})\Delta v(\mathbf{x})\,dS_{\mathbf{x}} + v^{(\mathrm{i})}(\xi)\,, \tag{21}$$

where $T^{+}(\mathbf{x},\boldsymbol{\xi})$ is the traction Green's function at point $\mathbf{x}$ on the illuminated side due to the application of a unit force at point $\boldsymbol{\xi}$ and $\Delta v(\mathbf{x})=v(\mathbf{x})^{(\mathrm{t})^+}-v(\mathbf{x})^{(\mathrm{t})^-}$ is the COD,

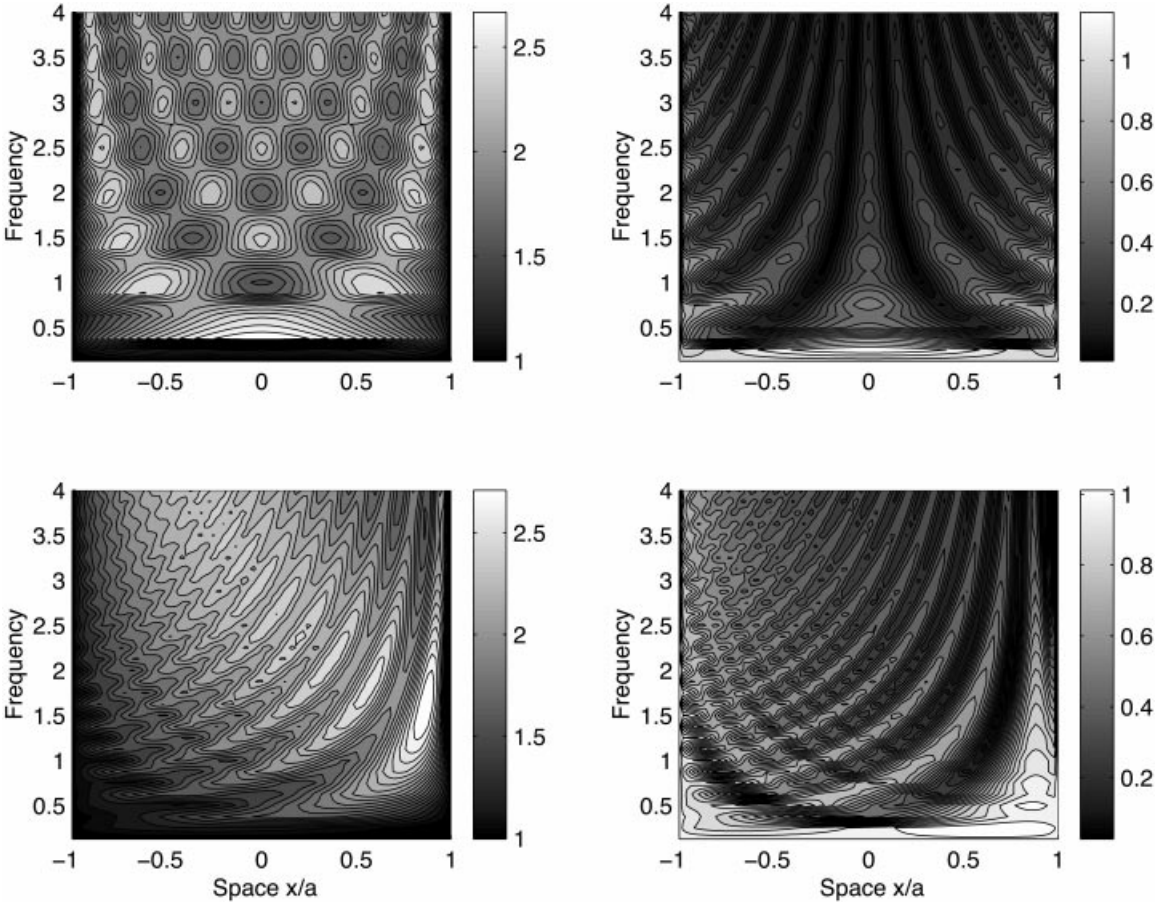

Figure 5. Contour map for incident angles $\gamma=0^\circ$, 30° (top and bottom), illuminated and shaded (left and right) sides. These (f–$\mathbf{x}$) diagrams display the total crack displacement amplitudes along the crack sides against the normalized frequency $\eta=\omega a/\pi\beta$.

which depends upon the *reflected* and *diffracted* fields only, i.e. $\Delta v(\mathbf{x}) = 2(v^{(r)^+}(\mathbf{x}) - v^{(d)^-}(\mathbf{x}))$. The subscript in the differential indicates the space variable over which the integration is performed.

The traction Green's function $T^+(\mathbf{x}, \boldsymbol{\xi})$ is given by

$$T^+(\mathbf{x}, \boldsymbol{\xi}) = \frac{ik}{4}\left(\frac{-\zeta}{r}\right) H_1^{(1)}(kr), \tag{22}$$

where $H_n^{(1)}(\cdot)$ is the Hankel function of the first kind, order n and $r_0 = \sqrt{\xi^2 + \zeta^2}$ is the distance between the receiver and the centre of the crack. Let $r = \sqrt{(x-\xi)^2 + \zeta^2}$ be the distance between the receiver and a point on the crack $\mathbf{x} = (x, 0)$, so that (for $x \ll r_0$)

$$r \sim r_0(1 - x\xi/r_0^2) \quad \text{and} \quad H_1^{(1)}(kr) \sim H_1^{(1)}(kr_0)\, e^{-ikx\cos\theta}. \tag{23}$$

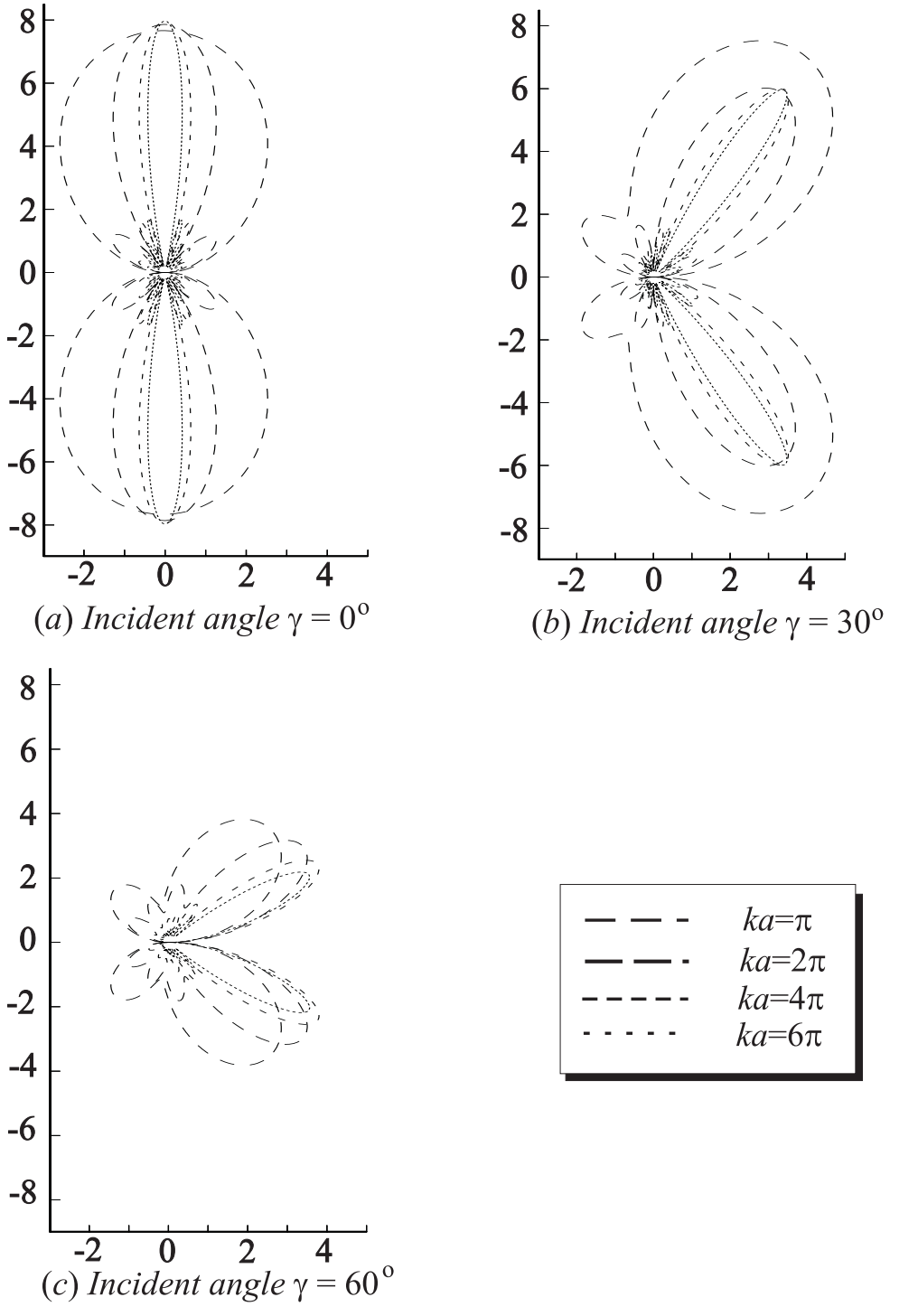

Figure 6. Scattered radiation far-field patterns for three incident angles. The amplitude of the total diffracted field is plotted for the cases of a plane wave impinging upon a crack for values of $ka = \pi$, 2π, 4π and 6π respectively. Receivers are located at a distance $2a$ from the origin. The number of lobes increases with frequency.

This implies that for a large r_0 a cylindrical wave can be represented as a plane wave in the neighbourhood of the crack. Hence the traction Green function $T^+(\mathbf{x}, \boldsymbol{\xi})$ can be approximated by

$$T^+(\mathbf{x}, \boldsymbol{\xi}) \sim \frac{ik}{4}\left(\frac{-\zeta}{r_0}\right) H_1^{(1)}(kr_0)\, \mathrm{e}^{-ikx\cos\theta}, \tag{24}$$

where (ξ, ζ) is the location of the receiver on the shaded side (see Fig. 1). Substituting eq. (22) into the first term of eq. (21), the full field can be approximated as

$$v^{(\mathrm{t})}(\xi) = \frac{-ik}{4} H_1^{(1)}(kr_0)\sin\theta \int_{-a}^{a} \mathrm{e}^{-ikx\cos\theta}\, \Delta v(\mathbf{x}) dS_{\mathbf{x}} + v^{(\mathrm{i})}(\xi). \tag{25}$$

In the far field the full diffracted waves given by the first term in eq. (5) can be viewed as a product of the radial function $H_1^{(1)}$, which depends on kr_0, and an angular function that depends on θ, ka and γ. Note that the COD $\Delta v(\mathbf{x})$, which depends on ka and γ, varies along the crack and contributes within the integral eq. (25) to define the angular modulation function. With the analytical solution the COD is easily computed at a very low computational cost. Radiation patterns can then be computed for various frequencies and incidence angles.

4 NUMERICAL RESULTS

In all numerical tests the finite crack is located within the interval $[-a, a]$. Fig. 5 shows contour maps of displacement amplitudes of $v^{(\mathrm{t})}$ given by eq. (21) for receivers located along the x-axis between $x=-a$ and $x=a$ on the illuminated side and on the shaded side (left and right respectively) versus frequency. The top figures correspond to an incident angle $\gamma=0^\circ$ and the bottom figures correspond to an incident angle $\gamma=30^\circ$. These (f–$\mathbf{x}$) diagrams display the total crack displacement amplitudes along the crack sides against the normalized frequency $\eta=\omega a/\pi\beta$. The symmetry in both geometry and excitation can be seen in the diagram for incident angle $\gamma=0^\circ$. For the illuminated (top left) side ($\gamma=0^\circ$), with increasing frequency the number of peaks increases following approximately an odd integer sequence. These peaks are weak and they show small fluctuations due to the little trapping of energy by the crack.

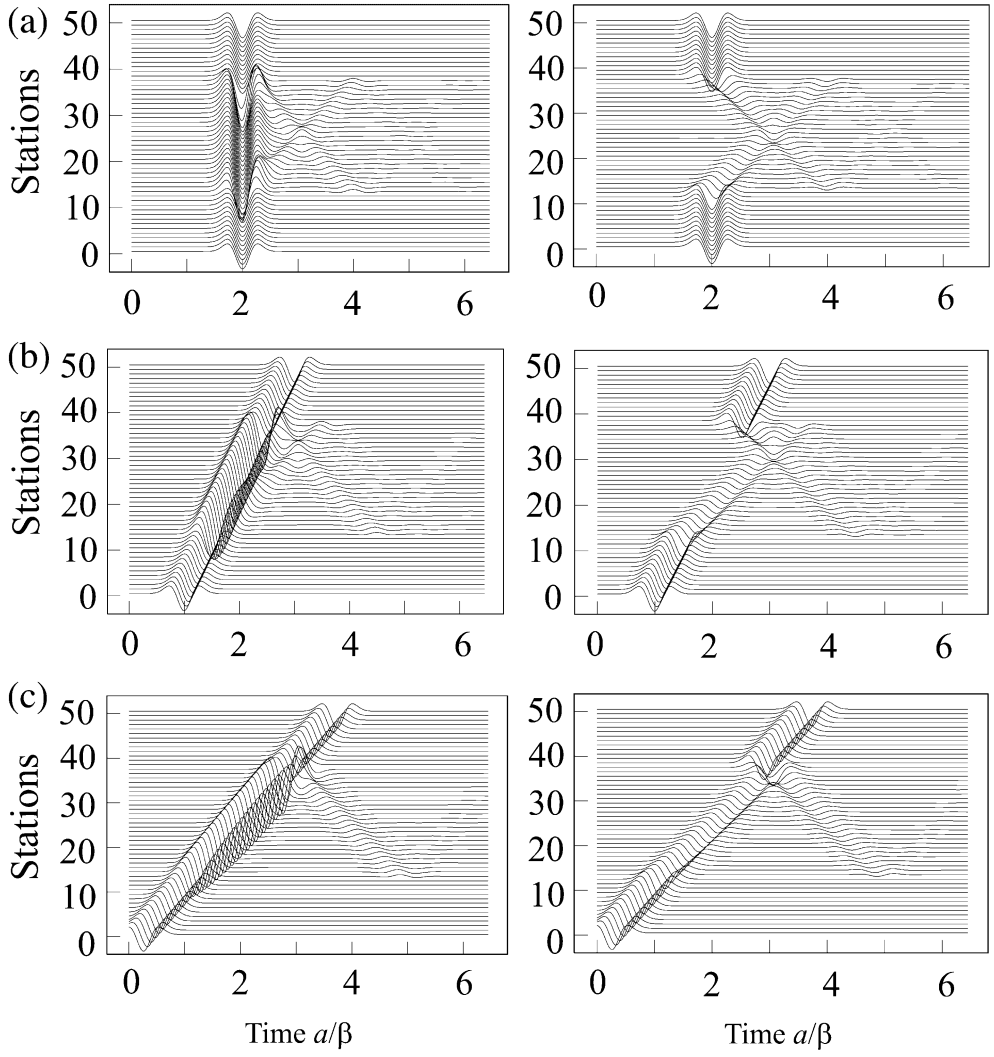

Figure 7. Synthetic seismograms for $\gamma=0^\circ$, 30°, 60° (top, middle and bottom figures, respectively) on the illuminated (left) and shaded (right) sides at 51 equally spaced receivers along the x axis. Receivers 13 to 37 are located on the crack. The incident time signal is a Ricker wavelet with characteristic period $t_{\mathrm{p}}=0.7\ a/\beta$.

For an incident angle $\gamma = 30^\circ$ (bottom left and right) the symmetry is lost. The interaction between lateral modes of oscillation results in progressive changes in the spectral alignment of the peaks along the profile of frequencies.

Scattered far-field radiation patterns for *SH* waves are shown in Fig. 6. The amplitude of the total diffracted field is plotted for the cases of a plane wave impinging upon a crack for values of $ka = \pi$, 2π, 4π and 6π respectively. Receivers are located at a distance $2a$ from the origin. A discretization of the crack has been used to solve the integral in eq. (25). The number of lobes increases with frequency. Radiation patterns provide information about how scattered waves are distributed in space for a given frequency and incident angle.

Synthetic seismograms are computed from frequency-domain results using a Fast Fourier Transform (FFT) algorithm. The traces correspond to the total field for receivers located along a line that contains the crack. The time variation of the incoming wavefield is a Ricker wavelet with characteristic period

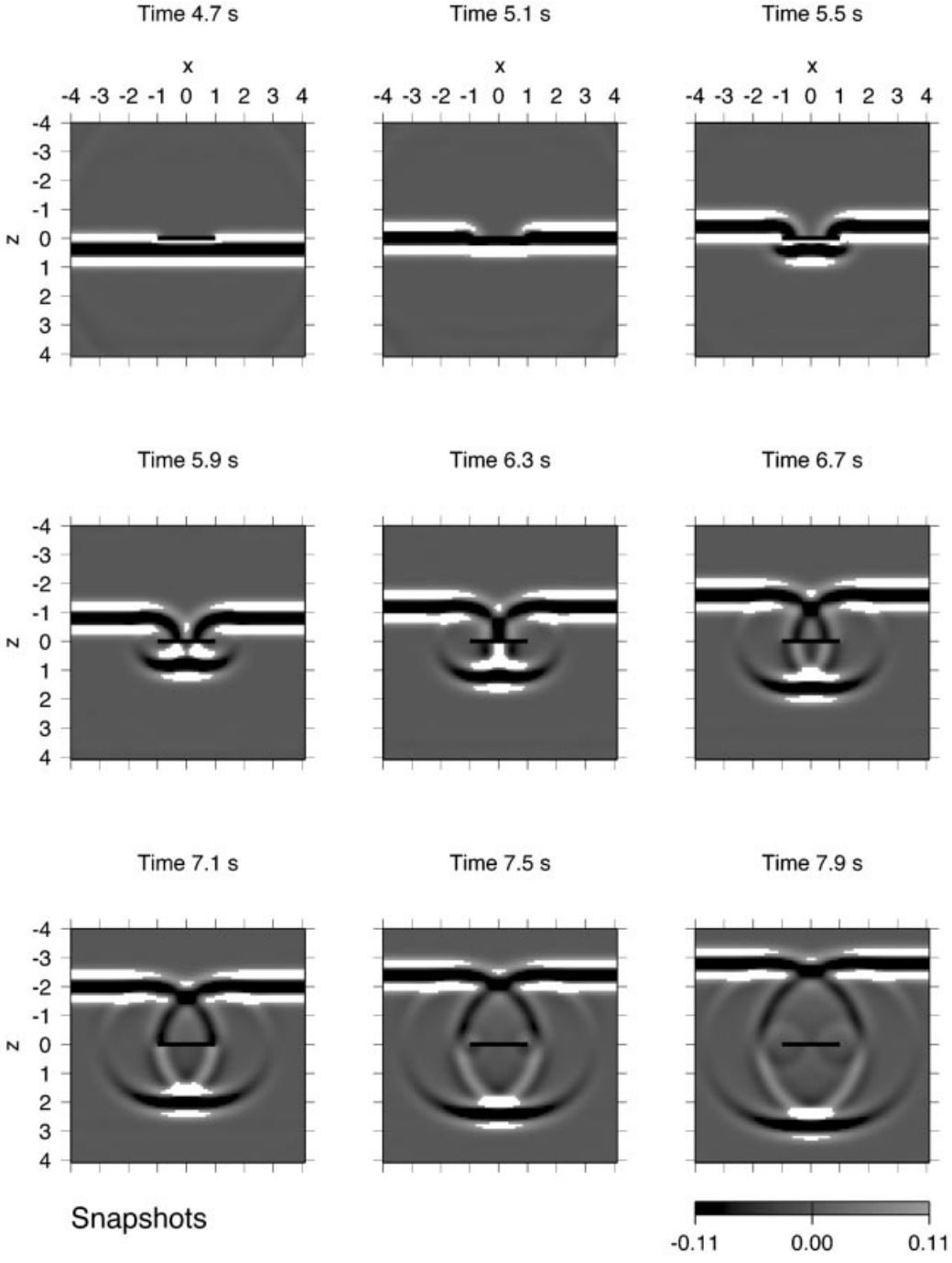

Figure 8. Snapshots for $\gamma = 0^\circ$ at nine different times. A square grid of 101×101 equally spaced receivers within a square of length $8a$. The crack is located at the centre of the square in the interval $(-a, a)$. The effect of diffraction on the shaded side creates a gap or a shadow. On the other hand, diffraction can be observed on the illuminated side. As time increases the wavefront recovers and the diffraction effect caused by the crack on the plane wave disappears. Greyscale slightly changed to enhance diffraction.

$t_p = 0.7\ a/\beta$. Fig. 7 shows the synthetic seismograms for both the illuminated and the shaded sides (left and right respectively) for incident angles $\gamma = 0^\circ$, 30°, 60° (a, b and c respectively). Results in time show that the incident wave is not present on the shaded side, and that it appears doubled on the illuminated side. The amplitude of the diffracted fields depends on the characteristic period of the Ricker wavelet and on the angle of incidence. The examples displayed correspond to wavelengths that are smaller than the crack length (about $0.7a$ for the predominant or characteristic frequency of excitation). For this relatively high frequency the diffraction is noticeable only for the first arrivals from the edges. Diffraction is significant at low frequencies and has to cancel out the so-called reflected field. In any event, the COD should be null at zero frequency.

Finally, in Fig. 8 we computed snapshots for a mesh with 101×101 equally spaced receivers located within a square of length $8a$. The crack is located on the interval $(-a, a)$. In these computations instead of using the far-field approximation for the traction Green's function $T^+(\mathbf{x}, \xi)$ we have used the expression for T^+ given in eq. (22). These results show how the plane wave reaches the crack and the diffraction caused at the edges of the crack degenerates the wavefront. The effect of diffraction on the shaded side creates a gap or a shadow. On the other hand, diffraction can be observed on the illuminated side. As time increases the wavefront recovers and the scattering effect caused by the crack on the plane wave diminishes.

5 CONCLUSIONS

We have constructed an analytical solution for the scattering and diffraction of *SH* waves by a finite crack. The solution has been obtained based upon the classical Sommerfeld approach for the half-plane screen. Based on a local approximation of cylindrical waves by plane waves and the symmetries at the edges and at both sides of the crack, diffracted waves are taken into account to constitute the complete solution. This enables us to include easily their contribution as explicit terms in the convergent series eq. (20) for the displacement field, leading to a virtually exact solution for the scalar case. This analytical solution is a powerful tool to study the effects of a single crack under the incidence of plane *SH* waves. It can be used to validate numerical methods, and opens up the possibility of studying scattering and diffraction of *SH* waves in a medium with multiple crack configurations. Since the goal of inversion of seismic reflection data is to retrieve a detailed image of the underlying geology and to quantify physical parameters, a further issue along these lines is to classify the response of single cracks with different sizes, orientations and frequencies to provide reliable models in the inversion process. In addition, the computation of this solution is very fast; this is a promising approach to numerous applications.

ACKNOWLEDGMENTS

We thank J. H. Spurlin, D. Komatitsch, M. Korn, R. Vai and F. Tilmann for their critical comments and remarks. Suggestions from an anonymous reviewer helped to improve the manuscript. This work has been partially supported by DGAPA-UNAM, México under grant IN104998, Instituto Mexicano del Petróleo under project D.1341 and CONACYT under project number NC-204.

REFERENCES

Abramowitz, M. & Stegun, I.A. (eds), 1970. *Handbook of Mathematical Functions,* Dover Publications, New York.

Achenbach, J.D., 1973. *Wave Propagation in Elastic Solids,* North-Holland, Amsterdam.

Achenbach, J.D. & Gautesen, A.K., 1986. Edge diffraction in acoustics and elastodynamics, in *Low and High Frequency Assumptions,* pp. 336–401, eds Varadan, V.K. & Varadan, V.V., Elsevier, Amsterdam.

Achenbach, J.D., Gautesen, A.K. & McMaken, H., 1982. *Ray Methods for Waves in Elastic Solids with Applications to Scattering by Cracks,* Pitman, London.

Aki, K. & Richards, P.G., 1980. *Quantitative Seismology,* W. H. Freeman, San Francisco.

Ang, D.D. & Knopoff, L., 1964a. Diffraction of vector elastic waves by a clamped finite strip, *Proc. Nat. Acad. Sci. USA,* **52,** 201–207.

Ang, D.D. & Knopoff, L., 1964b. Diffraction of vector elastic waves by a finite crack, *Proc. Nat. Acad. Sci. USA,* **52,** 1075–1081.

Banerjee, P.K. & Butterfield, R., 1981. *Boundary Element Methods in Engineering Science,* McGraw Hill, London.

Boersma, J., 1960. Computation of Fresnel integrals, *Math. Compt.,* **14,** 380.

Boström, A., 1987. Elastic wave scattering from an interface crack: antiplane strain, *ASME J. appl. Mech.,* **109,** 503–508.

De Hoop, A.T., 2000. Transient two-dimensional Kirchhoff diffraction of a plane elastic SH wave by a generalized linear-slip fracture, *Geophys. J. Int.,* **143,** 319–327.

Huang, J.Y., 1995. Interaction of SH-waves with a finite crack in half-space, *Eng. Fract. Mech.,* **51,** 217–224.

Hudson, J.A., 1986. A higher order approximation to the wave propagation constants for cracked solid, *Geophys. J. R. astr. Soc.,* **87,** 265–274.

Kraut, E., 1976. Review of theories of scattering of elastic waves by cracks, *IEEE. Trans. S. U.,* **3,** 162–167.

Loeber, J.F. & Sih, G.C., 1968. Diffraction of antiplane shear waves by finite crack, *J. acoust. Soc. Am.,* **44,** 90–98.

Macdonald, H.M., 1902. *Electric Waves,* Cambridge University Press, Cambridge.

Mow, C.C. & Pao, Y.H., 1971. The diffraction of elastic waves and dynamic stress concentrations, *US Air Force Project Rand,* Report R-482-PR.

Murai, Y., Kawahara, J. & Yamashita, T., 1995. Multiple scattering of *SH* waves in 2-D elastic media with distributed cracks, *Geophys. J. Int.,* **122,** 925–937.

Sommerfeld, A., 1949. *Optics,* Vol. IV, *Lectures on Theoretical Physics,* Academic Press, New York.

APPENDIX A: FUNCTION $F(z)$

Function W in eq. (4) can be represented by a Fresnel integral in terms of function $F(z)$ given in eq. (5). Here we discuss some properties of $F(z)$ needed to prove (in Appendix B) the convergence of series eq. (19). This function has the following property:

$$F(-z) = \sqrt{\pi}\, e^{-i(z^2 - \pi/4)} - F(z)\,. \tag{A1}$$

For the problem at hand, z is real-valued. In order to study the asymptotic behaviour of F for large arguments one has

$$F(z) = \frac{i}{2z} + O(z^{-3}) \quad \text{for } z \gg 0\,. \tag{A2}$$

Following the analysis in Achenbach & Gautesen (1986, p. 356) for $|z| \ll 1$, we obtain

$$F(z) = \frac{\sqrt{\pi}}{2} e^{i\pi/4} - z + O(z^2) . \tag{A3}$$

Function $F(z)$ can be written as

$$F(z) = \sqrt{\pi/2}\left\{ g(z\sqrt{2/\pi}) + i f(z\sqrt{2/\pi}) \right\} . \tag{A4}$$

We use the rational approximation for functions $f(x)$ and $g(x)$ given in Abramowitz & Stegun (1970, p. 302). Function $f(x)$ is given by

$$f(x) = \frac{1 + .926x}{2 + x(1.792 + 3.104x)} \tag{A5}$$

and $g(x)$ is given by

$$g(x) = \frac{1}{2 + x(4.142 + 3.492x + 6.670x^2)} . \tag{A6}$$

Other possible approximations for these functions can be derived by means of the τ-method of Lanczos given in Boersma (1960).

APPENDIX B: PROOF OF $|Z| < 1$

In order to ensure convergence of the series in eq. (19), we must prove that $|Z| < 1$. For an arbitrary ka we have

$$|F(z)| inf |Z| = \left| \frac{2}{\sqrt{\pi}} e^{2ika - i\pi/4} \right| \left| F(\sqrt{4ka}) \right| = \frac{2}{\sqrt{\pi}} \left| F(\sqrt{4ka}) \right| . \tag{B1}$$

Let us analyse the asymptotic behaviour of $|F(\sqrt{4ka})|$ when $ka \to 0$ and when $ka \to \infty$. On the one hand, eq. (A2) yields

$$\lim_{ka \to \infty} \left| F(\sqrt{4ka}) \right| = 0 . \tag{B2}$$

On the other hand, from eq. (A3) we obtain

$$\lim_{ka \to 0} \left| F(\sqrt{4ka}) \right| = \frac{\sqrt{\pi}}{2} . \tag{B3}$$

In addition, we note that $\kappa \in (0, \infty)$, hence for positive arguments the function $F(z)$ is bounded and is in fact monotonically decreasing. Therefore, the series in eq. (19) is convergent since $|Z| < 1$.